THE RELATIONSHIP BETWEEN STRUCTURAL AND TECTONIC EVOLUTION AND MINERALIZATION AT THE COLES HILL URANIUM DEPOSTI, PITTSYLVANIA COUNTY, VIRGINIA

John Wyatt

Thesis submitted to the faculty of the Virginia Polytechnic Institute and State University in partial fulfillment of the requirements for the degree of

MASTER OF SCIENCE
In
GEOSCIENCES

Committee Members:
Robert J. Bodnar, Co-Chairman
Richard D. Law, Co-Chairman
Joseph G. Aylor
William S. Henika

October 7, 2009
Blacksburg, Virginia

Keywords: uranium deposit, structure, tectonics, Coles Hill

THE RELATIONSHIP BETWEEN STRUCTURAL AND TECTONIC EVOLUTION AND MINERALIZATION AT THE COLES HILL URANIUM DEPOSIT, PITTSYLVANIA COUNTY, VIRGINA

John Wyatt

ABSTRACT

The role of structure and tectonics in the formation of hydrothermal ore deposits and the localization of high-grade mineralization associated with fractures is well documented. In this study we have characterized the structural setting associated with uranium mineralization in the Coles Hill uranium deposit by relating the observed metamorphic and structural features (mylonitic foliation and fractures) to regional tectonic activity.

Drill cores and outcrops observed in this study show that NE/SW oriented fractures appear to be related to Mesozoic movement along the Chatham Fault. NW/SE oriented fractures cross cut and offset the NE/SW oriented fractures by1 to 2 cm and therefore post-date the NE/SW oriented fractures. NW/SE fracture orientations and parallel to the NW/SE regional cross faults and are suggested to relate to the formation of the cross faults during post Triassic basin inversion. Uranium mineralization is located within horizontal to shallowly dipping fractures suggesting uplift and erosion to form possible tension veins.

The cross faults with NW/SE orientations created pathways in which uranium bearing hydrothermal fluids could migrate from the Triassic basin shales westward into the adjacent highly fractured crystalline rocks, precipitating uranium due to oxidation-reduction reactions.

ACKNOWLEDGEMENTS

First and foremost I would like to thank Virginia Uranium Inc. for funding my research and allowing access to data and resources during this study.

I thank the Geosciences Department for funding. I also thank the office staff and especially Connie Lowe for all her advice and hard work.

I thank the Virginia Museum of Natural History, Martinsville for allowing me access to research materials for this study and especially to Jason Lunze.

Special thanks to my committee members, Dr. Joesph G. Aylor, Mr. William S. Henika and Dr. Richard D. Law for all of their discussions that have improved this study.

I would like to thank my mother Carolyn Wyatt, my father Harold Wyatt and my brother Kevin Bennett for their support and prayers over the past year and half. My advisor, Dr. Robert J. Bodnar for his extensive knowledge and I am very grateful for his support and time.

I would like to thank all my fellow graduated students and friends for their help during the difficult times and especially, Christy Bernard, Theresa Detrie, Marilyn Duncan, Rosario Esposito, Samuel Fortson, John Gannon, Ellen Gilliland, Stephanie Humphries, Eric Kazlaukas, Lindsay Kolbus, Matthew Steele-MacInnis, Ann Maddox, Crystal Mayhew, Daniel Moncada, Kathleen McFadden, Nathan Reed, Aaron Reffett, Ben Roth, Pilar Lecumberri Sanchez, Majken Schimmel and Pavithra Sekhar.

Dedicated to Mindy Schweiger who has taught me courage and the true meaning of determination.

TABLE OF CONTENTS

TABLE OF FIGURES

INTRODUCTION

The important role of structure and tectonics in the formation of hydrothermal ore deposits is well documented (Baudemont and Fedorowich, 1996; Jianwei et al., 2002; Cox, 2005; Safonov et al., 2007; Ford and Blenkinsop, 2008). Of particular relevance to ore forming systems is the localization of high-grade mineralization associated with intersecting fractures (Baudemont and Fedorowich, 1996). In hydrothermal uranium deposits intersecting fractures may represent areas in which oxidizing fluids and reducing fluids mix to precipitate high-grade uranium mineralization (Craw, 2000; Cox, 2005). In this study we have characterized the structural setting associated with uranium mineralization in the Coles Hill uranium deposit and have related the observed metamorphic and structural features (mylonitic foliations and fracture sets) to regional tectonic activity.

The Coles Hill uranium deposit, located in south central Virginia in Pittsylvania County (Figure 1) is considered the largest undeveloped uranium deposit in the United States (Aylor et al., 2009). The Coles Hill uranium deposit is thought to be a hydrothermally derived deposit (Aylor et al., 2009) that is associated with major regional scale structural and tectonic features. To better understand the origin of the deposit a detailed structural study of outcrops, drill core and hand samples was conducted to determine the relative chronology of the structural and tectonic events and their possible relationship to mineralization.

GEOLOGICAL EVOLUTION IN THE VICINITY OF COLES HILL AND WESTERN PIEDMONT

The earliest tectonic event associated with formation of the southern Appalachians is the breakup of the supercontinent of Rhodina at about 670 to 640 Ma. to form the Iapetus Ocean (Carter et al., 2006). During the subsequent closing of the Iapetus Ocean at about 550 Ma, a westward inclined subduction zone formed and produced a volcanic arc along the east coast of Laurentia, which is now part of present day North America (Gates, 1981; Carter et al., 2006). As subduction continued and Iapetos closed a volcanic arc collided with continental North America and this mountain building event is known as the Taconic Orogeny (540 to 440 Ma) (Gates, 1981; Hibbard et al., 2003; Carter et al., 2006). Today the Basset and Fork Mountain formations form the Smith River Allochthon in southern Virginia (Conley et al., 1973). The Smith River Allochthon is approximately 250 km long and approximately 50 km wide (Carter et al., 2006) and the Coles Hill deposit is located on its eastern edge (Figure 2). The western boundary of the Smith River Allochthon is represented by the Bowens Creek Fault and it is bounded on the east by the Chatham Fault (Hibbard et al., 2003). The Smith River Allochthon forms a thin skinned sheet like structure that has been thrust westward along the Ridgeway fault (Carter et al., 2006). Generally, the Bassett Formation consists of quartzo-feldspathic biotite gneiss, amphibolite and quartzite, and the Fork Mountain Formation comprises biotite paragneiss, aluminous mica schist, quartzite, calcsilicate rocks and amphibolite (Henika, 2002).

Intrusion of plutons of the Rich Acres Gabbro and the Leatherwood Granite of the Martinsville Igneous Complex into the Smith River Allochthon occurred at 464 to 457 Ma (Lineberger, 1983). The dominant fabric in these rocks is a metamorphic mylonitic foliation that strikes NE/SW. This metamorphic foliation is contemporaneous with the Alleghanian Orogenty

and possibly the Brookneal Shear Zone (Gates, 1981), however we are unable to determine if there is a genetic link between foliation and the Brookneal Shear Zone. For simplicity, in the discussion to follow we correlate the timing of foliation with the formation of the Brookneal Shear Zone during the Alleghanian Orogoney (350 Ma.) (Gates, 1981; Lineberger, 2003). During continued closing of the Iapetus Ocean, at 375 Ma, Avalonia collided with Laurentia resulting in the Acadian Orogeny (Henika et al., 1981; Hibbard et al., 2003). Finally, during the Carboniferous at 350 to 300 Ma, Gondwana collided with Laurentia to produce the supercontinent of Pangaea and a third mountain building event known as the Alleghanian Orogeny (Hibbard et al., 2003). Foliation associated with the Alleghanian Orogeny formed sub-parallel to the previously developed foliation in the Leatherwood (Gates, 1981).

During the Mesozoic, from 250 to 130 Ma, the NE/SW trending Danville Triassic basin formed as a result of the eventual break up of Pangaea, when the present day Atlantic Ocean was formed (Figure 2) (Hibbard et al., 2003). The basin fill is composed of shales, siltstone, sandstones and conglomerates (Henika et al., 1981). Before erosion to the present day land surface the Triassic basin sediments may have extended westward to the Bowens Creek Fault. During later westward-directed plate motion, the Triassic basin underwent a process known as basin inversion that created a topographical high on the eastern edge of the basin (Schlische et al., 2002) and hydraulic gradients from east to west that would promote the migration of fluids towards the Chatham Fault. Evidence of uplift along Mesozoic basins was documented north of Coles Hill in the Taylorsville basin as indicated by faster cooling of the eastern edge of the basin then the western edge (Tseng et al., 1999). This suggested fluid flow from the east to the west (Tseng et al., 1999). Mesozoic diabase dikes and cross faults were interpreted to be associated with contraction of the Mesozoic basins (Tseng et al., 1999). This event produced the present day

dips of sedimentary units (40 to 50° NW). The uplift and erosion has created the narrow sub-basin as we see it today (Schlische et al., 2002). The present day geometry is also consistent with the presence of listric faults.

The Chatham Fault is the major structural feature in the Coles Hill area that separates the metasedimentary rocks of the Smith River Allochthon, mylontized gneiss and the Leatherwood granite of the Martinsville Igneous Complex to the west from the Triassic basin to the east (Figures 2) (Gates, 1981; Hibbard et al., 2003). The Chatham Fault is a normal fault that strikes 030° - 040° and dips at 60° to the SE. During the Mesozoic rifting event, cataclastic activation of the Chatham Fault is evidenced by truncation of the Triassic rocks in the Danville basin (Henika et al., 1981; Lineberger, 1983;). The Frith Fault (parallel to the Chatham Fault) is recognized as a boundary between cataclasite and protocataclasite associated with deformation along the Chatham Fault and coarse mylonites, protomylonties and amphibolites associated with the Martinsville Igneous Complex (Lineberger, 1983). Thinning of the crust as a result of rifting opened pathways for emplacement of vertical Jurassic diabase dikes striking N-S (Lineberger, 1983) (Figure 3). Post Jurassic strike-slip motion along the Chatham Fault is evidenced by offsets in Jurassic diabase dikes that cross the Chatham Fault, documented by Marline in magnetic maps. Movement on regional scale faults oriented approximately parallel and perpendicular (cross faults) to the Chatham Fault also continued after Jurassic time based on Jurassic diabase dike offsets by approximately a 100 meters shown on magnetic contour mapping in the Coles Hill area and regional geologic mapping (Gates, 1981) and exploration bore hole mapping for the near-by Leesville Dam (Nelson, 1959).

METHODS

In this study the structural setting associated with uranium mineralization in the Coles Hill deposit has been characterized. To accomplish this, structural discontinuities, including mylonitic foliation and multiple fracture orientations were measured in outcrops and drill core (Figure 4). Structural trend discontinuity orientations were obtained and reported in azimuth 0 - 180°.

Five large pavement outcrops (Figures 4,5) were selected, and these are located at different distances from the two major structural features in the Coles Hill area, namely the Chatham fault and cross faults that are oriented perpendicular to the Chatham Fault. This approach was used to test whether structural discontinuities at Coles Hill could be related to these major structural events and if the intensity of fractures varies as a function of distance from the Chatham Fault and/or cross faults. Outcrop fracture orientations were examined to test for relationships with the major structural features in the area. Only strikes were measured in outcrops. Outcrop SPG 223 near the Frith House was located in the mylonitic gneiss unit and approximately 20 meters from the nearest surface exposure of one of the cross faults and 400 meters from the nearest surface exposure of the Chatham Fault. Outcrop GTA 894 in the mylonitic gneiss within Whitethorn Creek was located 300 meters from the nearest surface exposure of a cross fault and 20 meters from the surface exposure of the Chatham Fault.

Outcrop SPG 223 (Figure 5) was a relatively flat surface consisting of mylonitic gneiss believed to be derived from Leatherwood Granite (Henika et al., 1981) and measures approximately 5 meters by 10 meters. Following washing with high-pressure water to remove vegetation and other debris, six 50 cm by 50 cm windows were selected for detailed analysis (Figure 6). The windows were chosen to include all structural discontinuities in the outcrop. The

orientation of every discontinuity (fractures, planes of foliation, and orientations of quartz veins) within each window was measured. Windows 1 and 2 contain few fractures but many foliation planes were observed and measured. Windows 3 and 4 contain high densities of both fractures and foliation planes. Windows 5 and 6 contain abundant unltramylonite and quartz veins and fractures.

Outcrop GTA 894 also consisted of mylonitic gneiss believed to be derived from Leatherwood granite (Henika et al., 1981) and measured approximately 3 by 5 meters. Owing to the smaller size of outcrop GTA 894 the entire outcrop was selected and every observable structural feature was measured, including fractures, quartz veins and foliation planes.

Three outcrops (Figures 4,5) in the Triassic basin were also studied and these were located at various distances from the Chatham Fault. Every structural discontinuity observed within a 5 by 5 meter square was measured. Outcrops SPG 231, SPG 311 and MA 771 (Figure 5) are located less than 1 km, approximately 2 km and approximately 3 km, respectively, from the surface expression of the Chatham Fault.

During an earlier exploration program in the 1980's, Marline Inc. (Marline, 1982), drilled 12 oriented core holes at Coles Hill. Structural discontinuities, including fractures, foliation and quartz veins were measured in three drill cores from this earlier exploration program. The drill holes selected were along a transect that crossed the southern ore body and extended from the crystalline rocks west of the Chatham Fault and across the Chatham Fault into the Triassic basin. Drill core 41-190 is located 500 meters west of the Chatham Fault and is collared within the mylonitic gneiss unit in the southern ore body. Drill core 41-193 is collared approximately within the surface expression of the Chatham Fault and becomes progressively more distant from the Chatham Fault with depth. Drill core 57-27 is collared in the Triassic sedimentary rock and

drilled at an angle of 53° so that the hole crosses the Chatham Fault at a vertical depth of approximately 39.5 meters (100 meters of drill core length) and extends into the crystalline rocks west of the Chatham Fault.

The orientations of mylonitic foliations and fractures in drill cores were measured along the entire length of the core, except where core had been removed and destroyed during assaying by Marline Inc. Because the drill holes were not drilled vertically (i.e., perpendicular to the surface), the orientation had to be corrected in order to record the correct structural orientations with respect to geographic coordinates. The drill cores were all drilled with an azimuth of 028° and this orientation had been marked on the core during drilling. To return the orientation to vertical, the core was placed into a Styrofoam holder that was attached to the center of a non-metallic table on which compass directions had been marked (Figure 7). The Styrofoam holder was inclined at the angle of the drill holes. Each piece of drill core was inserted into the Styrofoam holder, the azimuth was set at 028°, and the angle of the core was set at either 52° (cores 41-190 and 41-193) or 53° (core 57-27). Then, the orientations of structural discontinuities were measured and these orientations represented the orientations of these features after correcting for plunge and trend of the drill core.

Data were plotted on either equal area 2% contour maps (drill core) or rose-diagrams (outcrops) using RockWare StereoStat. Strikes and dips were manually entered into excel like spreadsheets composed of columns. A negative sign was entered for dips to the south otherwise the program assumes a north dip. Then the poles to the planes were calculated and contoured at 2%. Rose-diagrams for outcrops were done by entering the data in the same spreadsheet but without dips.

RESULTS

Fracture orientations and foliation planes in drill core and outcrops were measured to test whether these structural features correlate with regional structural trends defined by the Chatham Fault, Brookneal Shear Zone or cross faults in the vicinity of Coles Hill.

In drill core 41-190, the dominant set of fractures strikes 030° and dips 60° to the SE (Figure 8). A less abundant set of fractures strikes 130° and dips about 80° degrees to the SW (Figure 8). Foliation orientations show a similar pattern with a dominant foliation striking 035° and dipping about 60°SE (Figure 9). Both the foliation and the fracture orientations are similar to the strike of the Chatham Fault and Brookneal Shear Zone, both of which strikes approximately 030° and dip 60° to the SE (Gates, 1981; Jerden, 2001).

Drill core 41-193 also shows a dominant fracture set striking 030° and dipping about 60° to the SE (Figure 8). Unlike core 41-190, the less abundant set of NW striking fractures is not present in this core (Figure 8). The foliation shows a dominant strike direction of 020° and dip of 60° SE (Figure 9). Again, these structural orientations are similar to the strike of the Chatham Fault and Brookneal Shear Zone.

Drill core 57-27 is collared in and passes through 100 meters of Triassic sedimentary rocks before reaching the crystalline rocks beneath the Chatham Fault. Fractures in the crystalline rocks are oriented 070° and dip 70° SE (Figure 8). Fracture orientations in the Triassic rocks in this drill core strike 120 - 130° and dip 60° to the SW (Figure 8) and are similar to fracture orientation in Triassic rocks measured away from the Chatham Fault (Figure 10). A few horizontal fractures, are also observed in this core (Figure 10). A third set of fractures in this drill core strikes approximately E-W and is steeply dipping. The NW/SE strikes of fractures in the Triassic are similar to the cross faults (Figure 3).

Outcrop SPG 223 shows a dominant NW/SE fracture orientation (Figure 8). This strike is different from the dominant NE/SW fracture orientation observed in drill cores. Outcrop SPG 223, which is located 20 meters from a cross fault, shows a dominant fracture orientation that is more closely related to the cross faults than to the Chatham Fault.

Outcrop GTA 894 is located near the Chatham Fault and contains 17 fractures striking NE/SW, similar to the strike of the Chatham Fault. Outcrop GTA 894 shows a dominant NW/SE fracture orientation (Figure 8).It is important to note that the NW/SE fractures related to basin inversion (Schlische et al., 2002), cross cut and are later than the NE/SW fractures that correspond to the strike of the Chatham Fault and Brookneal Shear Zone. Foliation orientations within the two outcrops are similar and strike 040 - 050° (Figure 9). Moreover, only one foliation strike was observed in each of these outcrops. As a result, only a few representative measurements of foliation were obtained from each outcrop.

Fracture orientations from all three Triassic outcrops, SPG231, SPG 311 and MA 771, have a dominant NW/SE strike (Figure 10). Outcrops SPG 231 and SPG311 also show a NE/SW fracture pattern that resembles the trend of the Chatham Fault. The number of NE/SW fractures decreases as the distance from the Chatham Fault increases. For example SPG 231 (Figure 10) contains 17 fractures out of 87 (~20%) that strike 030°, whereas in outcrop SPG 311, located 2 km from the Chatham Fault, only 6 (out of 45 fractures measured (~13%) strike 030° (Figure 10). The outcrop most distant from the Chatham Fault (MA 771) contained no fractures striking 030° (Figure 10).

INTERPRETATION

The dominant foliation observed at Coles Hill was produced during possible ductile movement (Gates, 1981). The foliation strikes NE/SW and predates the Chatham Fault, recording earlier possible ductile movement during the Alleghanian Orogeny (350 Ma) (Gates, 1981). The foliation represents the oldest structural feature recorded in the study area (Gates, 1981).

The dominant fracture orientation in drill cores 41-193 (Figure 9) and 41-190 (Figure 9) strikes approximately 030° and dips 60° SE are similar to the strike of the Chatham Fault. Core 57-27, which passed through about 100 meters of Triassic rocks, shows a dominant NW/SE fracture strike and the fractures are steeply dipping. These fractures are likely related to the same tectonic event that caused the continued post Jurassic fault movement (Nelson, 1959; Gates, 1981). Also, only a limited portion of the non-Triassic core 57-27 could be studied because some of the core was not oriented and other parts had been removed previously for assaying. Only sixteen fracture measurements could be made in the Triassic portion of core 57-27 (Figure 10).

Outcrops of mylonitic gneiss (SPG 223 and GTA 894) (Figure 8) showed a dominant NW/SE striking fracture set that cross cuts the NE/SW fracture set seen in the drill core. NE/SW fracture sets are offset by NW/SE fractures by 1 to 2 cm indicating that the NW/SE fractures post-date the NE/SW fractures. The fracture offset is attributed to post Jurassic movement on the sub-vertical cross faults (Nelson, 1959; Gates, 1981), which strike similarly NW/SE perpendicular to the Chatham Fault. Outcrop SPG 223 (Figure 8), which is located 300 meters from the Chatham Fault, has only 5 fractures out of 96 fractures with orientations similar to the Chatham Fault (Figure 9). Outcrop GTA 894 (Figure 8), which is located 20 meters from the Chatham Fault contained 9 fractures out of 61 fractures that can be related to the Chatham Fault

(Figure 9). It is clear that the intensity of Chatham Fault related fractures decreases with distance from the fault.

The three outcrops in the Triassic basin, SPG 231, SPG 311 and MA 771 (Figure 10), have a dominant NW/SE fracture set strikes approximately 120° and a less abundant 030° striking set. Starting from outcrop SPG 231, which is closest to the Chatham Fault and moving eastward away from the fault, the number of fractures that have a NE/SW strike decreases to zero. We conclude that movement along the Chatham Fault continued after formation of the Triassic basin (Henika et al., 1981). Also the NW/SE fracture set, as previously seen in the mylonitic gneiss unit, cross cuts and post dates the NE/SW Chatham Fault related fractures, indicating that these fractures were active in post Triassic times.

Mineralized fractures studied by Marline Inc. and provided by Virginia Uranium Inc. strike E/W with horizontal to shallow dips (Figure 11) (Marline, 1982). These fractures likely were opened during uplift and erosion.

Cross fault related fractures were not seen in drill core because the drill holes parallel the cross faults but are seen in outcrops within the mylontized gneiss and Triassic. NE/SW fractures that parallel the Chatham Fault could predate the Triassic because of the low density of NE/SW fractures seen within the Triassic or could be a factor of distance of the first Triassic outcrop (1km) is too far from the Chatham Fault to see a high density. Horizontal fractures were not seen within the mylontized gneiss drill core because the fractures would be at the breaks within the core in the core boxes. Judging wither a break was a foliation plane or a fracture would be difficult and thus was not done.

In a time sequence, the mylonitic foliation striking 030° and dipping 60°, and observed in each drill core and outcrop in the mylonitic gneiss unit, is the oldest measured structural feature

observed at Coles Hill (Gates, 1981). During Mesozoic time the Triassic sedimentary rocks were deposited over the Smith River Allocthon and may have extended westward as far as the Bowens Creek Fault (Gates, 1981). The Bowens Creek Fault was active during Mesozoic extension and has been traced NW into the Scottsville Triassic basin (Gates, 1981). The Chatham Fault was active after Triassic deposition as Triassic facies belts have been folded and truncated along the fault (Gates, 1981; Thayer and Henika, 1981). During this time the 030° dipping 60° SE fracture set is thought to have formed (Figure 12). As opening of the Atlantic continued the Triassic Basin was uplifted on the east side to produce an inverted basin topography called basin inversion (Schlische et al., 2002). As the crust continued to thin, Jurassic diabase dikes were formed and cross faults oriented perpendicular to the Chatham Fault were formed (Gates, 1981; Schlische et al, 2002). The NW/SE striking fracture set reflects the cross faulting event (Figure 12). Unloading during erosion and uplift led to the opening of horizontal fractures that host uranium mineralization (Figure 10).

The sequence of events described above led to pathways, (i.e. the cross faults), from the Triassic basin into the amphibolite-bearing mylonitic gneiss unit. The topographic high (Schlische et al., 2002) produced by Triassic basin inversion created a hydraulic gradient in which hydrothermal fluids migrated westward into the amphibolite bearing mylonitic gneiss unit transporting uranium into the complex fracture network where the uranium was deposited due to oxidation-reduction reactions (Figure 12).

REFERENCES CITED

Aylor, J., Beard, J., Bodnar, R., 2009. Coles Hill, Chatham, Virginia uranium deposit. Geological Society of America Abstract. 41, 48.

Baudemont, D., Fedorowich, J., 1996. Structural Control of Uranium Mineralization at the Dominique-Peter Deposit, Saskatchewan, Canada. Economic Geology 91, 855-874.

Carter, B., Hibbard, J., Tubrett, M., Sylvester, P., 2006,. Detrital zircon geochronology of the Smith River Allochthon and the Lynchburg Group, southern Appalachians: Implications for Neoproterozoic- Early Cambrian paleogeography. Precambrian Geology, 1-26.

Conley, F., and Henika, W., 1973, Geology of the Snow Creek, Martinsville East, Price, and Spray Quadrangles: Virginia Division of Mineral Re- sources Report of Investigations 33, 71.

Cox, S, 2005. Coupling between Deformation, Fluid Pressures, and Fluid Flow in Ore-Producing Hydrothermal Systems at Depth in the Crust. Economic Geology 100th Anniversary Volume, 39-75.

Craw, D., 2000., Fluid flow at fault intersections in an active oblique collision zone, Southern Alps, New Zealand. Journal of Geochemical Exploration 69-70, 523-526.

Ford A., Blenkinsop T., 2008. Combining fractal analysis of mineral deposit clustering weights of evidence to evaluate patterns of mineralization: Application to copper deposits of the Mount Isa Inlier, NW Queensland, Australia. Ore Geology Reviews 33, 435-450.

Gates, A., 1981. Geology of the western boundary of the Charlotte belt at Brookneal, Va., Masters Thesis, Virginia Tech.

Heinrich, C., 2007. Fluid-fluid interactions in magmatic-hydrothermal ore formation. Minearalogical Society of America 65, 363-387.

Henika, W., Thayer, P.,1981, Geologic map of the Spring Garden Quadrangle, Virginia. Virginia Division of Mineral Resources 48, scale 1:24,000.

Henika, W., 2002, Geologic map of the Virginia portion of the Danville 30x60 minute quadrangle: Virginia Division of Mineral Resources Publication 166, , scale 1:100,000.

Hibbard, J., Stewart K., Henika, W., 2000. Framing the Piedmont Zone in North Carolina and Southern Virginia. Fieldtrip Guide book for the 50th SE GSA meeting, Geological Society of America, Raliegh, 1-26.

Hibbard, J., Tracy, R., Henika, W., 2003. Smith River allochthon: A southern Appalachian peri-Gondwanan terrane emplaced directly on Laurentia?. Geology March, 215 – 218.

Jerden, J., 2001. Origin of uranium mineralization at Coles Hill, Virginia (USA) and its natural attenuation within an oxidizing rock-soil-groundwater system. Ph.D. Thesis, Virginia Tech.

Jianwei, L., Meifu, Z., Xianfu, L., Zhaoren, F., Zijin, L., 2002. Structural control on uranium mineralization South China: Implications for fluid flow in continental strike-slip faults. Science in China 45, 851-864.

Lineberger, D.,1983. Geology of the Chatham Fault Zone, Pittsylvania County, Virginia. Masters Thesis Chapel Hill U.N.C.

Marline Inc., 1982. Mineralized Fracture Study Report, Coles Hill, Pittsylvania County, Virginia.

Nelson, W., 1959. Final geological report on the lower development of the Smith Mountain Combination Hydroelectric Project Mt. Airy Dan Site on the Roanoke River, Virginia. Appalachian Power Company, October 1959.

Safonov, Y., Gorbunov, G., Pek, A., Volkov, V., Zlobina, T., Kravchenko, G., Malinovsky, E., 2007. Structure of ore fields and deposits: current status and outlook for further development. Geology of Ore Deposits, 5, 343-371.

Schlische, R., Withjack, M., Olsen, P., 2002. Relative Timing of CAMP, Rifting , Continental Breakup, and Basin Inversion: Tectonic Significance. American Geophysical Union Monograph 1-28.

Tseng, H., Burruss, R., Onstott, T., Omar, G., 1999. Paleofluid-flow circulation within a Triassic rift basin: Evidence from oil inclusions and thermal histories, Geological Society of America Bulletin, February 1999. 275-290.

Virginia Division of Mineral Resources, 1993, Geologic Map of Virginia with expanded explanation: Virginia Department of Mines, Minerals and Energy 1:500,000 scale, 80.

Figure 1. Location map of the Coles Hill uranium deposit.

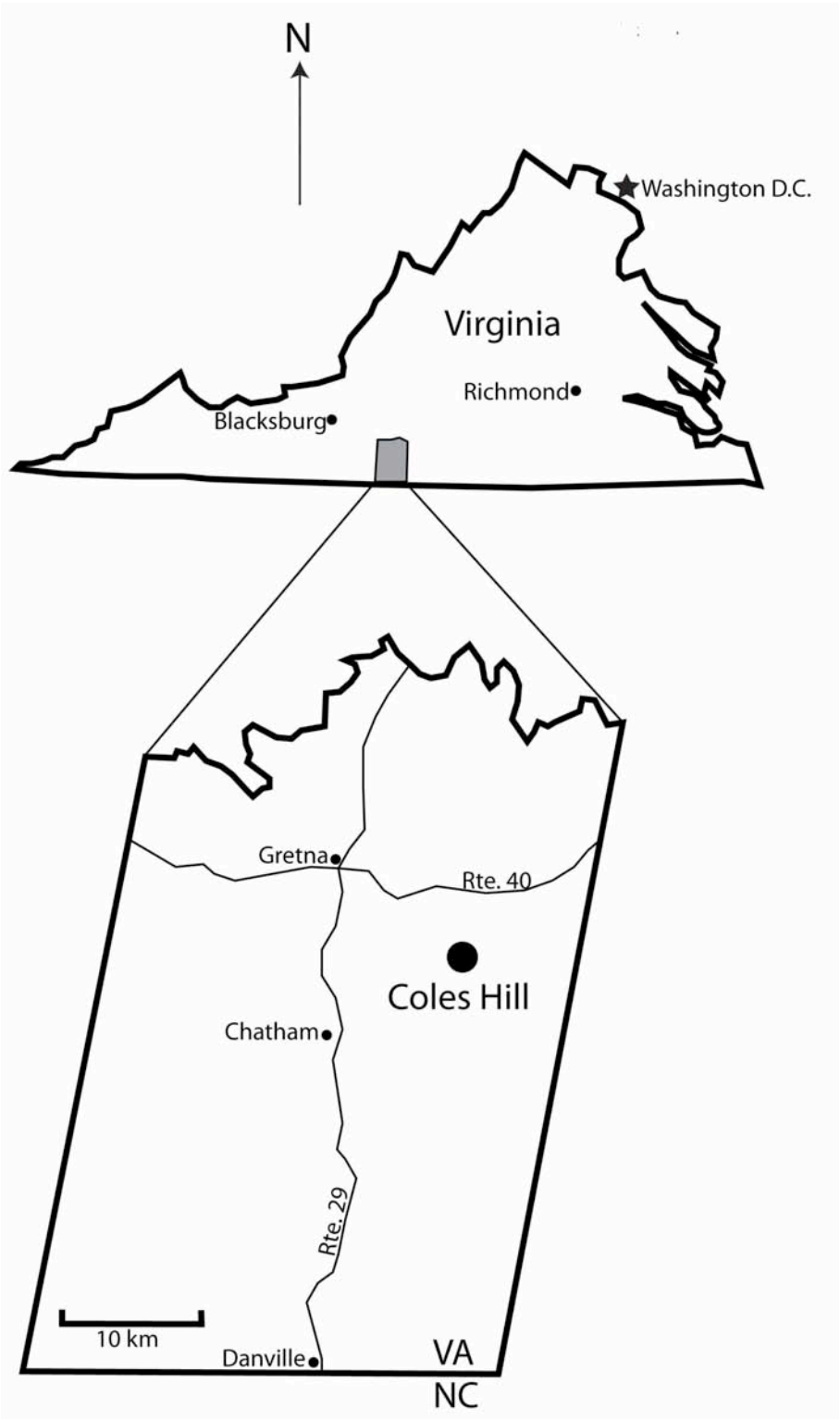

Figure 2. Simplified geological map showing the Bowens Creek Fault (BC), Chatham Fault (CF) and major lithotectonic units in the vicinity of Coles Hill. Map modified from Virginia Division of Mineral Resources (1993) and Henika et al. (1981)

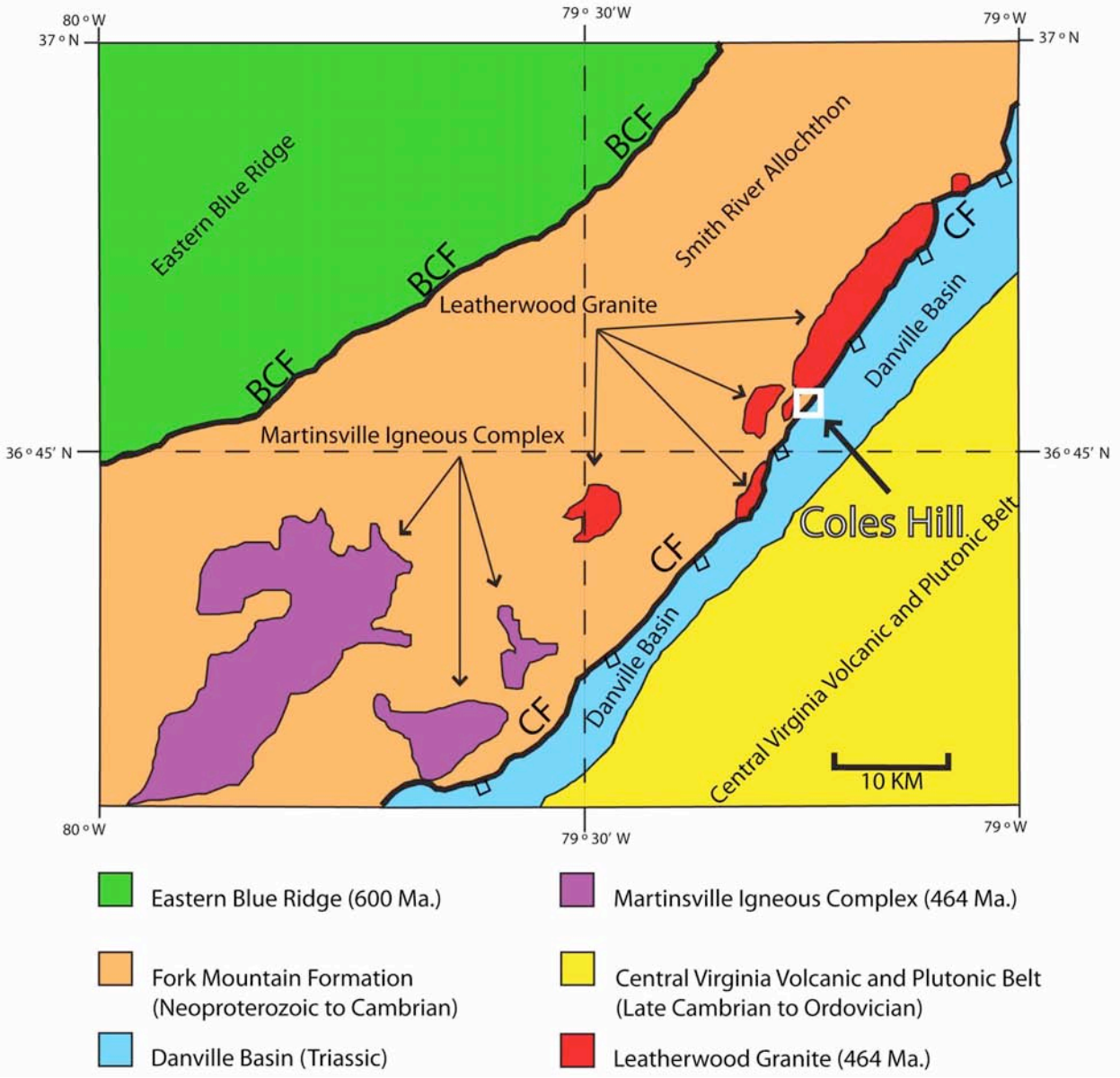

Figure 3. Simplified geological map in the immediate vicinity of Coles Hill showing the location of the north (N) and south (S) ore bodies. Map modified from Henika et al. (1981).

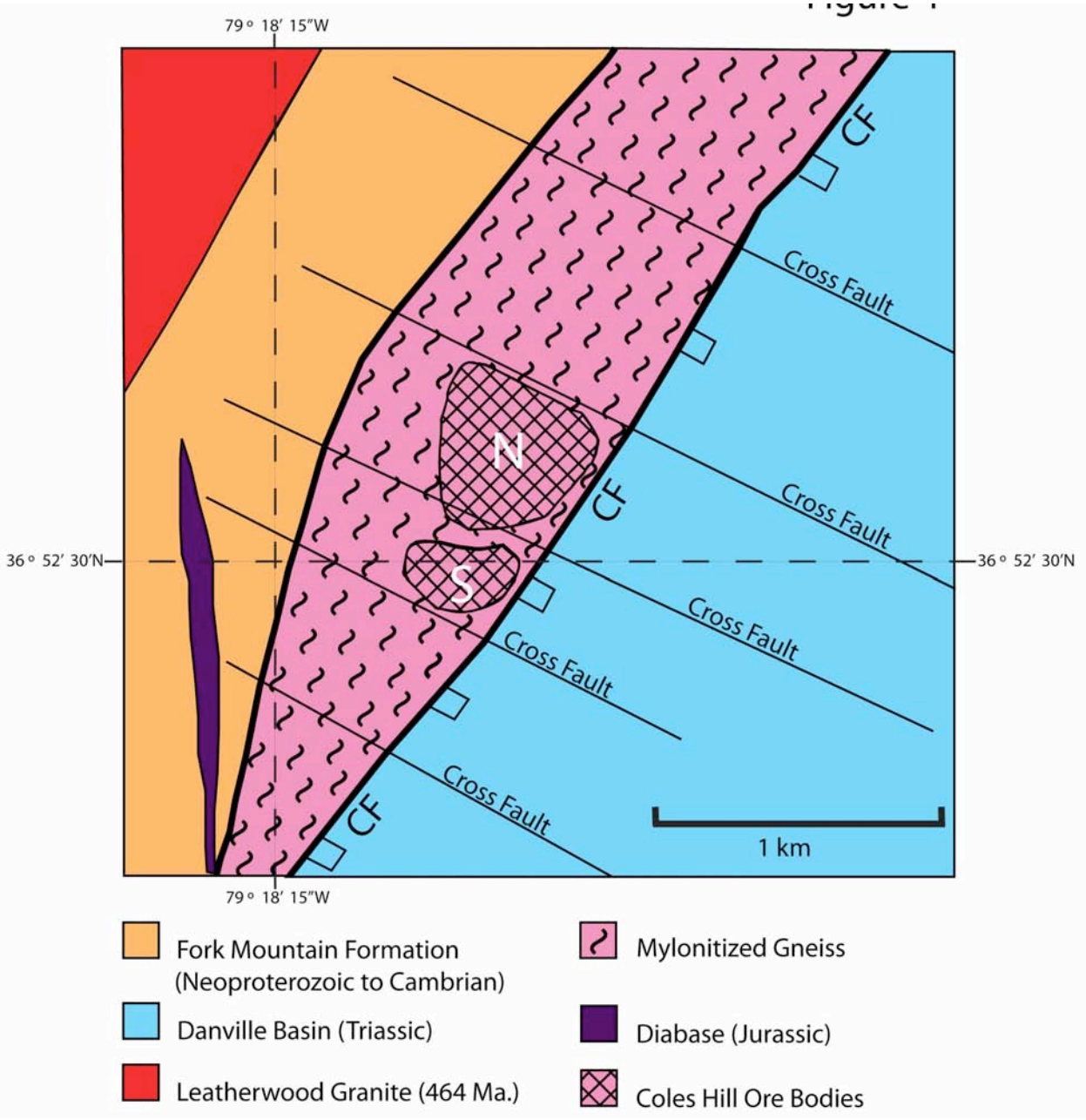

Figure 4. Regional geological map showing the locations of three drill holes and five outcrops. Map modified from Henika et al. (1981).

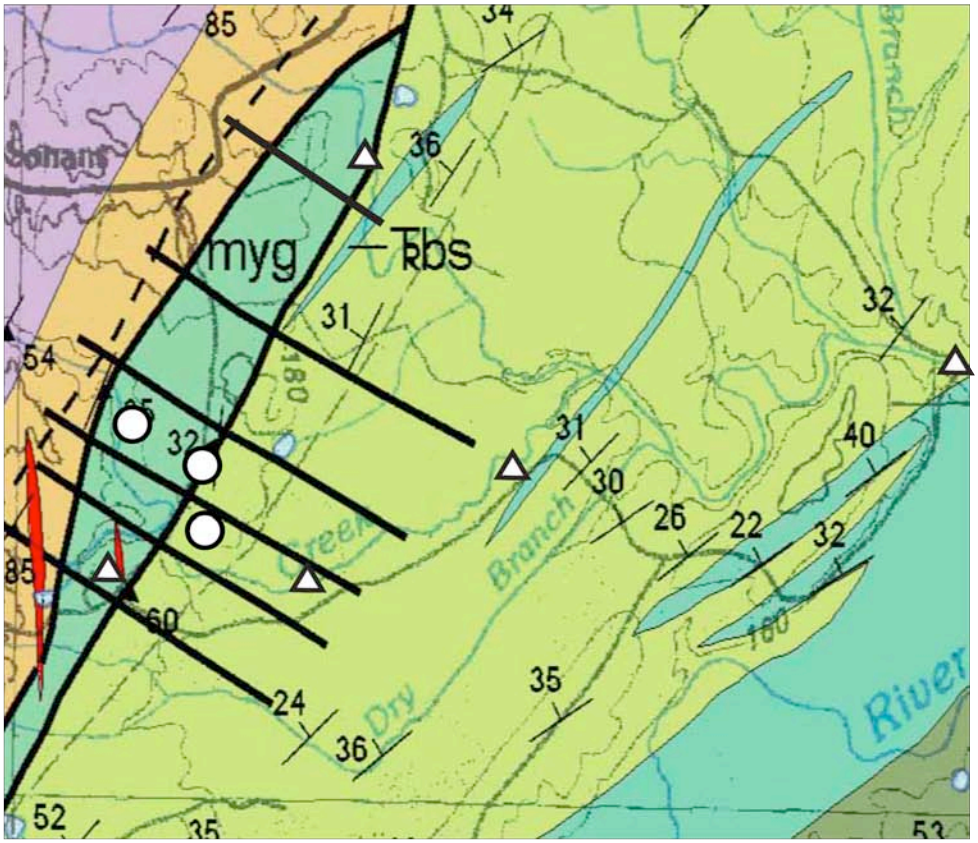

Figure 5. Photographs of five outcrops showing the dominant fracture strikes represented by blue (NW) and red (NE) tape. SPG 223 (N 36°51.991' W 79°18.718') and GTA 894 (N 36°52.333' W 79°16.9021') are located within the mylonitized gneiss. SPG 231 (N 36°52.322' W 79°17.976'), SPG 311 (N 36°52.322' W 79°16.843') and MA 711 (N 36°52.618' W 79°14.895') are located within the Triassic basin. Map image copyright by Google Earth (2009), copyright Europa Technologies (2009) and copyright Commonwealth of Virginia (2009).

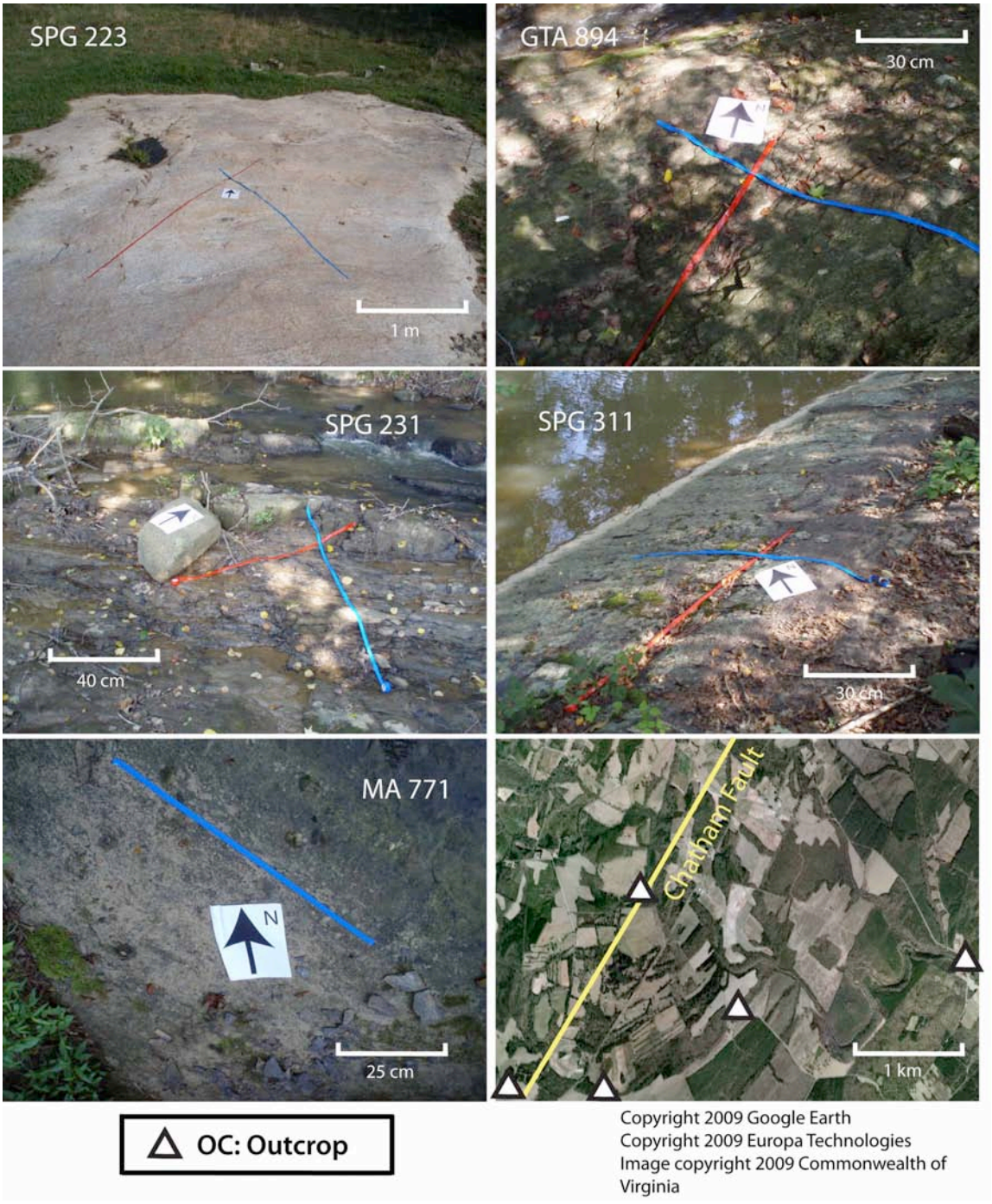

Figure 6. Photographs of 6 windows in outcrop SPG 223 in which structural features, such as fractures and foliations, were observed and measured. Each window (W1-W6) measures approximately 50 x 50 cm.

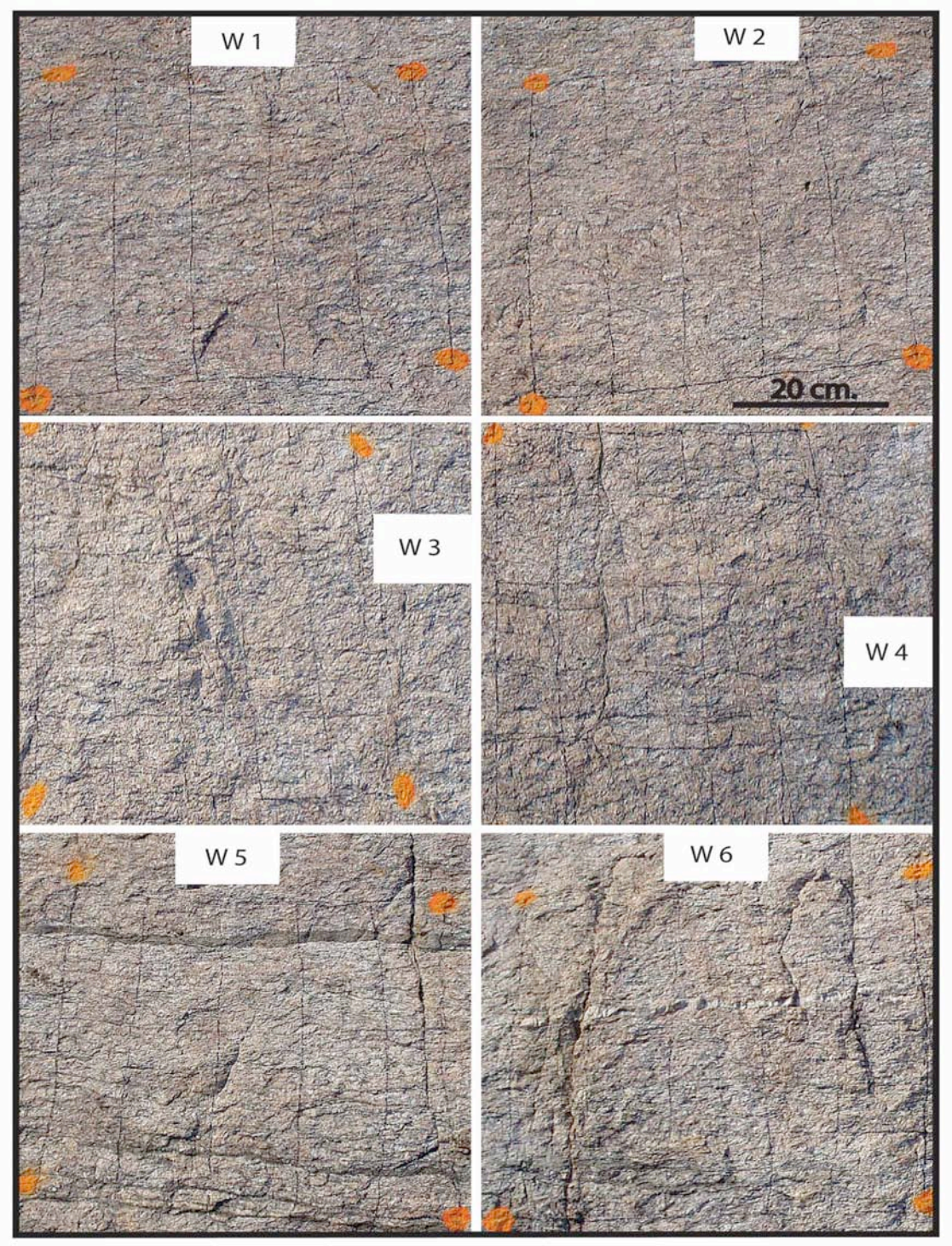

Figure 7. Photograph of apparatus used to correct angled drill core to a vertical position in order to obtain the correct strike and dip of fractures and foliations.

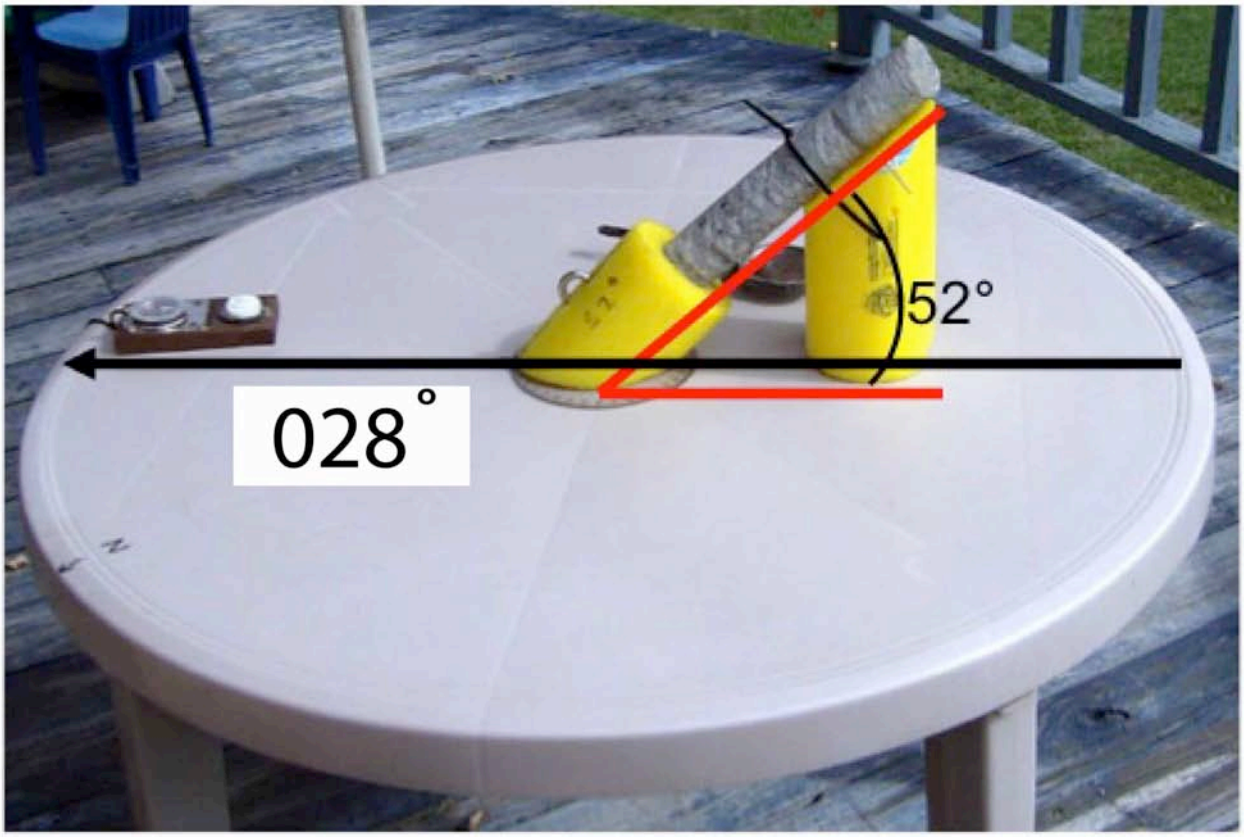

Figure 8. Photograph showing the location of two outcrops and three drill cores. Contour maps of poles to fracture strikes and dips are shown for drill cores 41-193, 41-190 and 57-27. Rose diagrams show fracture strikes for outcrops GTA 894 and SPG 223. Map image copyright by Google Earth (2009), copyright Europa Technologies (2009) and copyright Commonwealth of Virginia (2009).

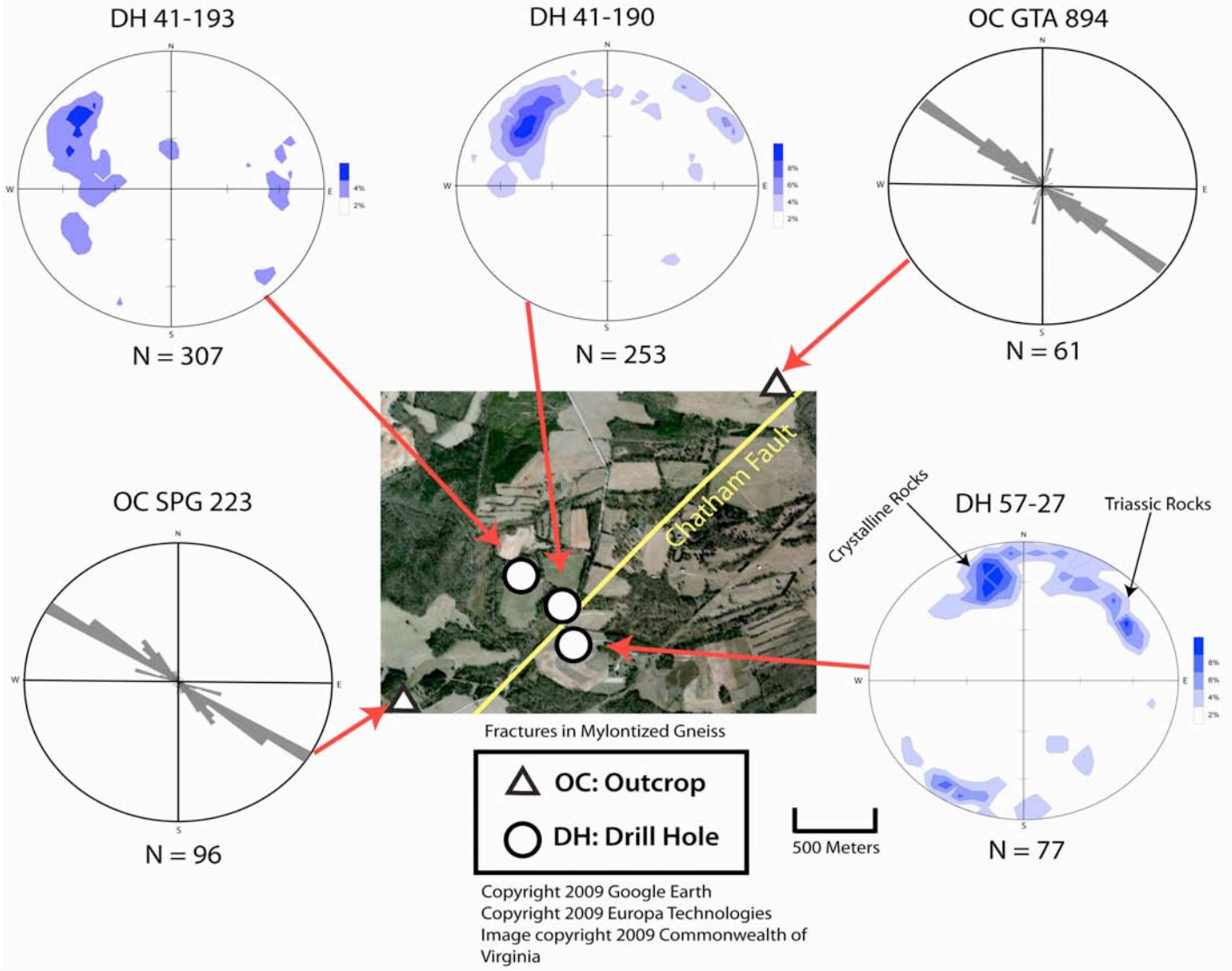

Figure 9. Photograph of outcrops and drill core location. Contour maps of poles to foliation planes for drill cores 41-193 and 41-190 and rose diagrams of GTA 894 and SPG 223 are shown. Image copyright by Google Earth (2009), copyright Europa Technologies(2009) and copyright Commonwealth of Virginia (2009).

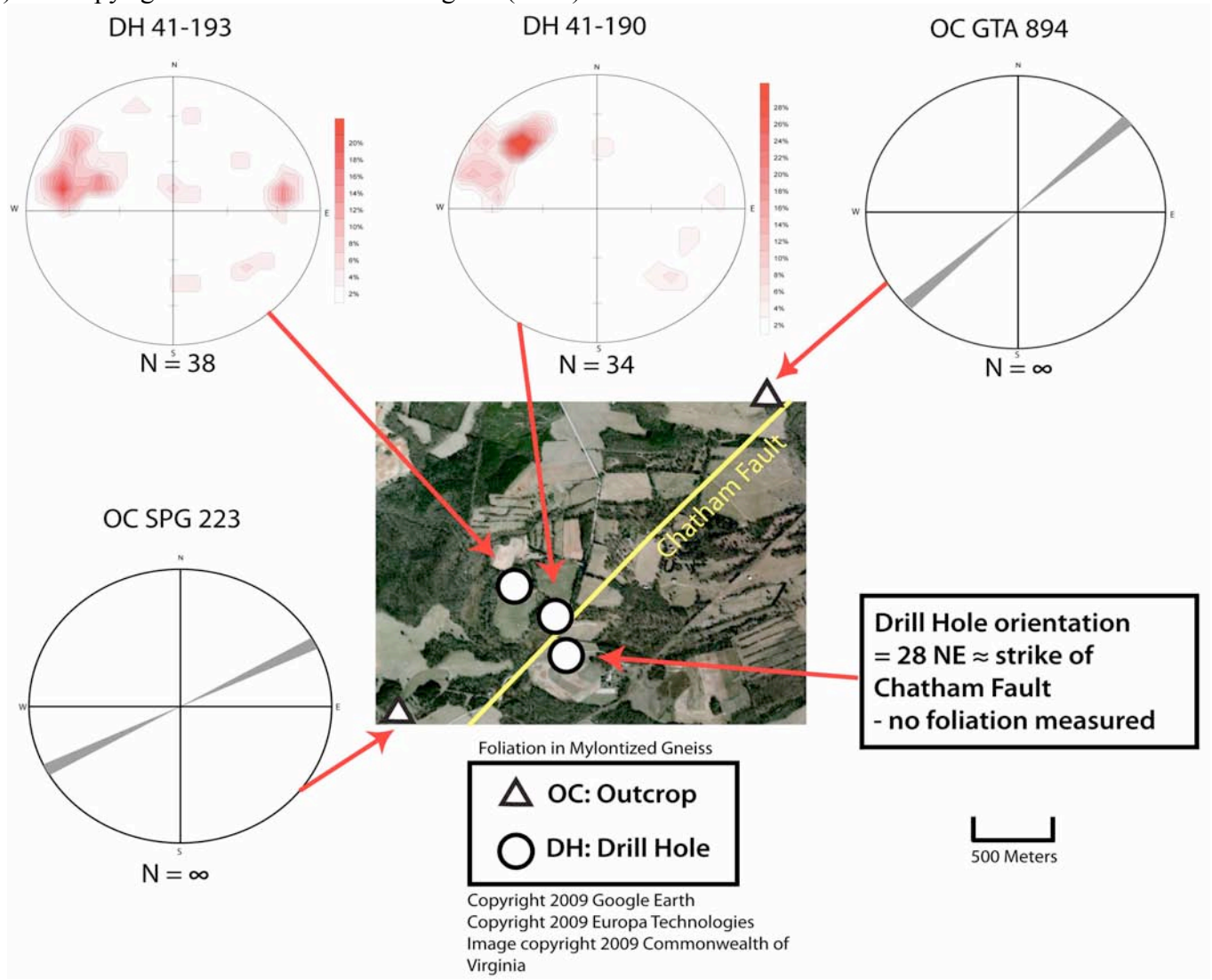

Figure 10. Photograph of Triassic outcrops and drill core 57-27. Contour map of poles to fracture strikes and dips of the Triassic sedimentary rocks from drill core 57-27 and rose diagrams of outcrops SPG 231, SPG 311 and MA 711 in the Danville Triassic basin are also shown. Image copyright by Google Earth (2009), copyright Europa Technologies (2009) and copyright Commonwealth of Virginia (2009).

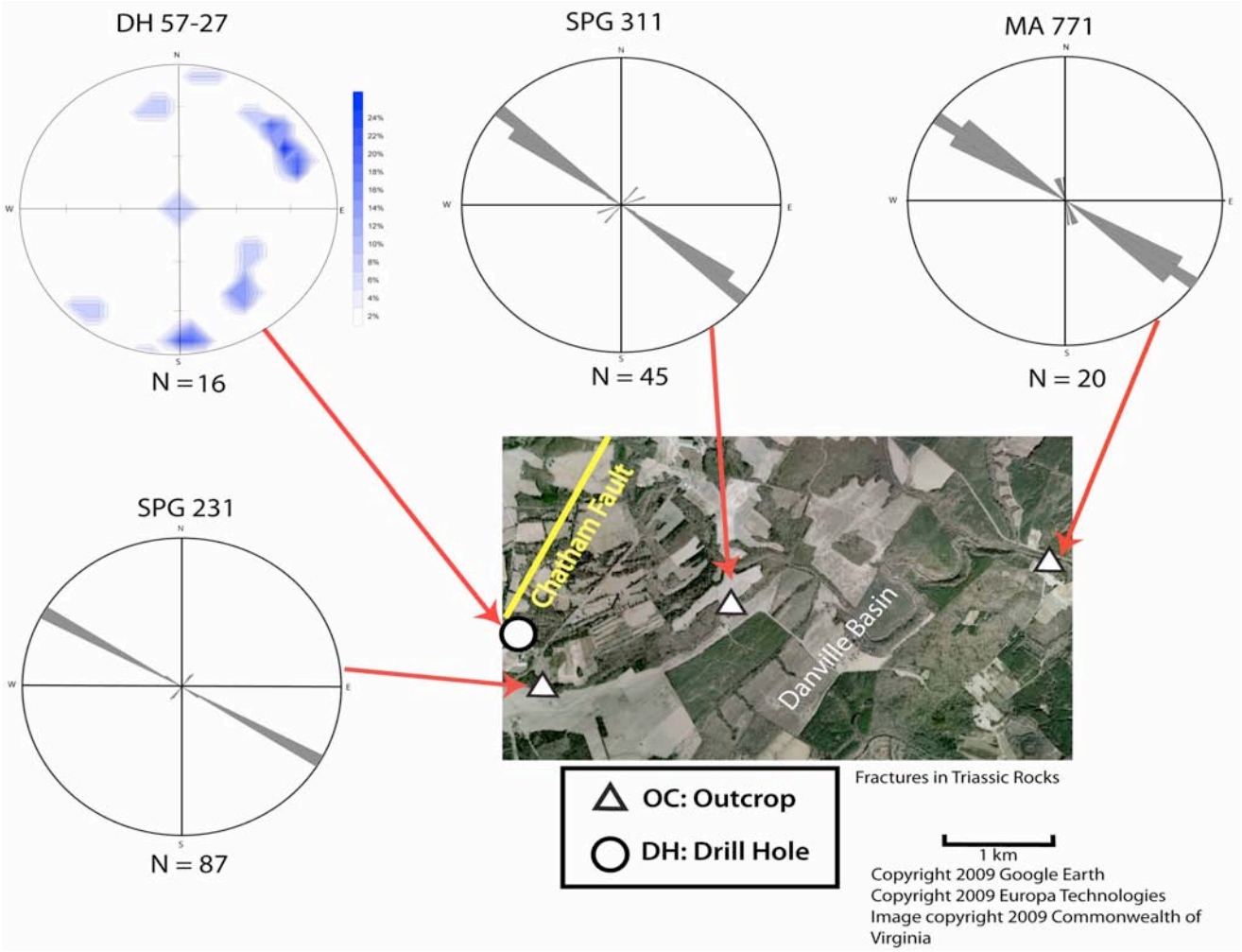

Figure 11. Contour diagram of poles to strikes and dips of uranium mineralized fractures collected by Marline Inc. and provided by Virginia Uranium Inc. Image modified from Marline Inc. (1981).

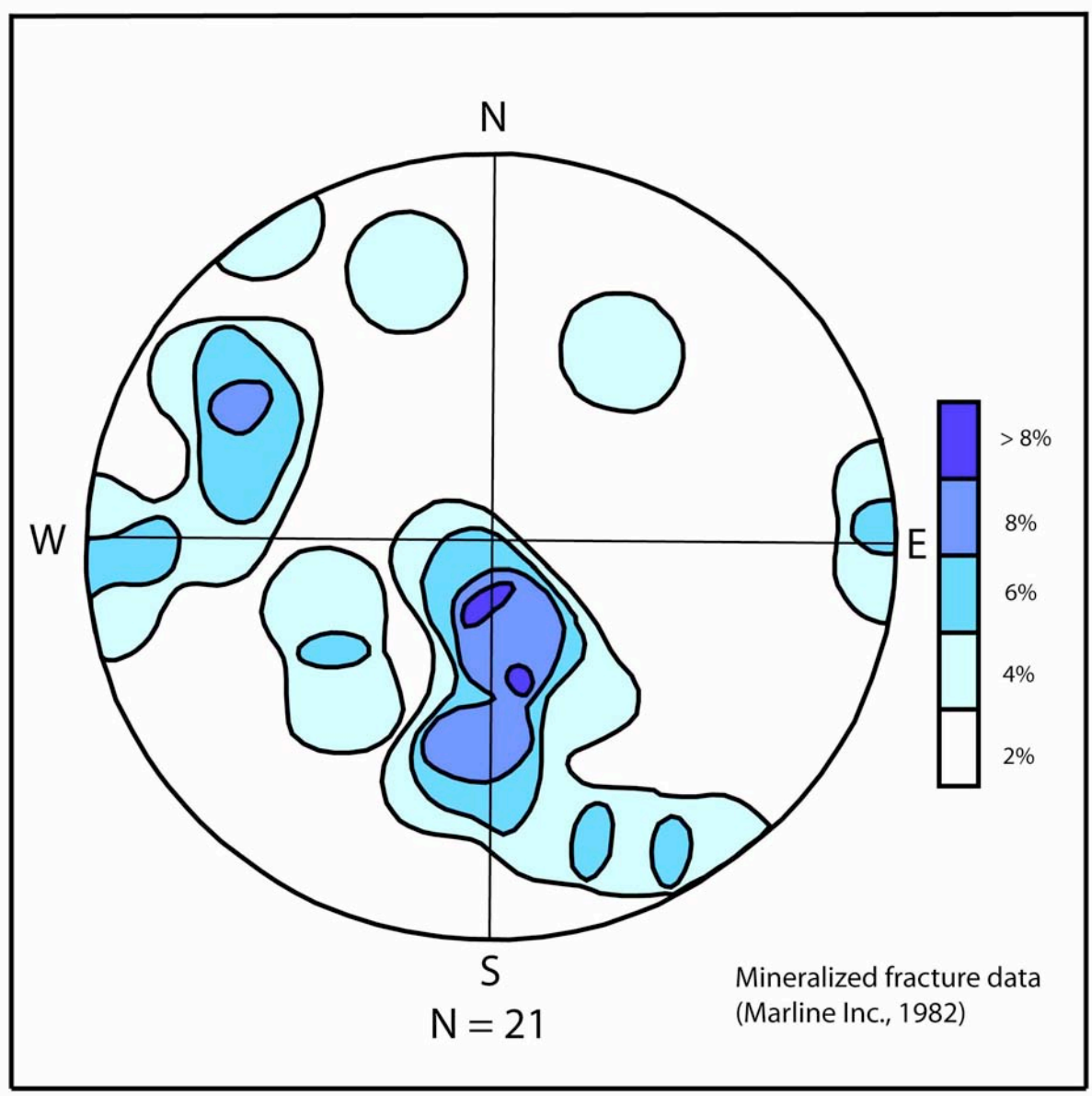

Figure 12. Schematic block diagrams showing simplified geological relationships in the vicinity of Coles Hill during the Alleghanian Orogeny, the Jurassic and at the present time.

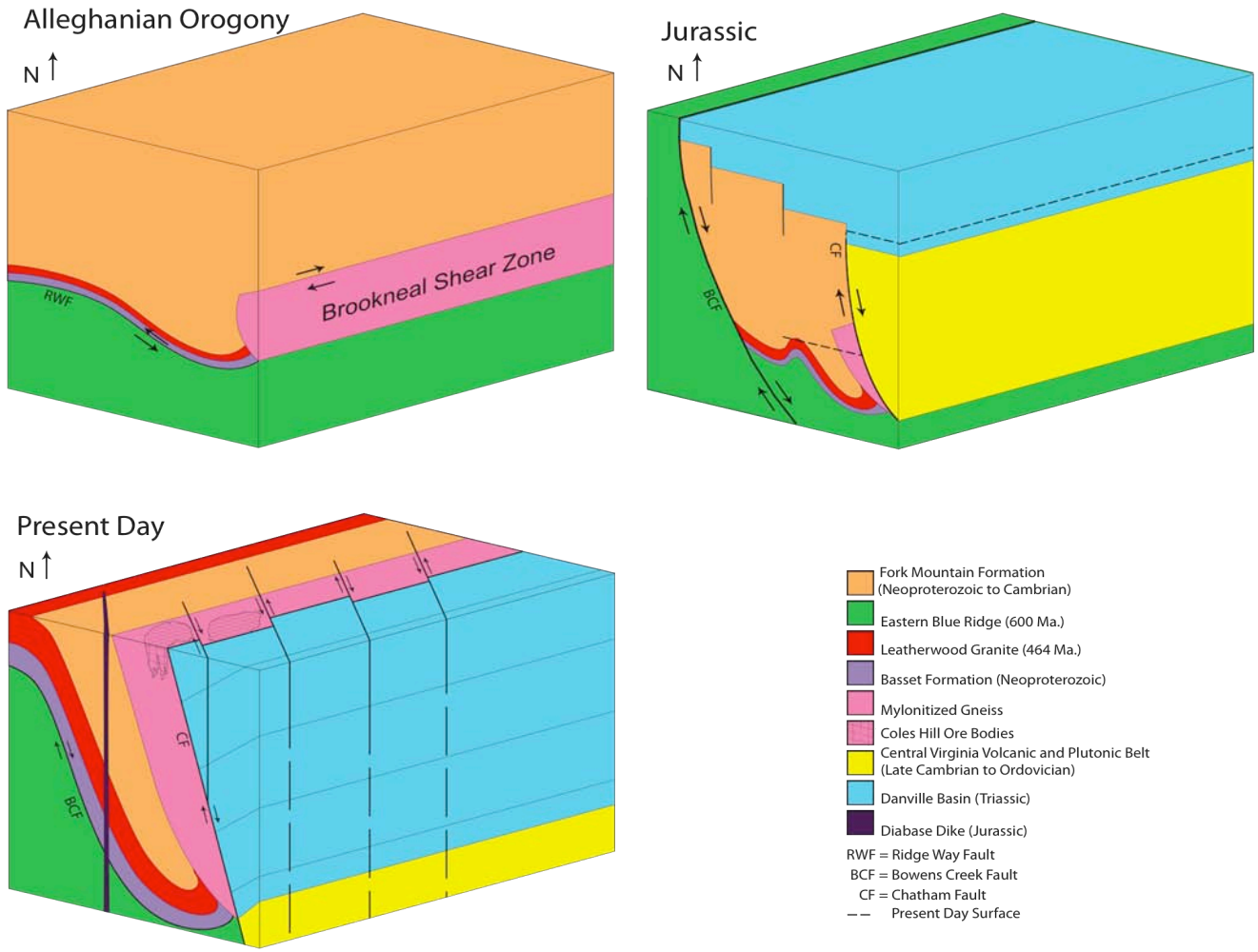

Appendix A

Foliation Orientation Measurement Data from Drill Core 41-193.

Depth (feet)	Strike	Dip	Direction	Comments
87 to 96.7	96	40	S	Crystalline
96.7 to 105.7	22	56	N	Crystalline
105.7 to 114.3	41	58	S	Crystalline
114.3 to 123.1	40	64	S	Crystalline
123.1 to 131.8	4	62	S	Crystalline
131.8 to 140.4	50	54	N	Crystalline
149.6 to 159.1	46	64	N	140.4 to 149.6 Unoriented
159.1 to 168.3	17	72	S	Crystalline
168.3 to 177.2	30	80	S	Crystalline
177.2 to 186.3	174	72	S	Crystalline
186.3 to 195.2	17	80	S	Crystalline
195.2 to 204.6	20	80	S	Crystalline
204.6 to 214.0	36	78	S	Crystalline
214.0 to 223.0	58	62	S	Crystalline
223.0 to 279.0	19	78	S	223.0 to 279.0 Brecciated
279.0 to 288.2	38	70	S	Crystalline
288.2 to 297.7	36	86	S	Crystalline
297.7 to 306.9	15	60	S	Crystalline
306.9 to 316.1	22	66	S	Crystalline
316.1 to 325.7	21	67	S	Crystalline
325.7 to 335.1	15	56	S	Crystalline
335.1 to 344.3	45	60	S	Crystalline
344.3 to 353.7	42	62	S	Crystalline
353.7 to 363.0	47	68	S	Crystalline
363.0 to 372.3	60	64	S	Crystalline
372.3 to 381.7	52	62	S	Crystalline
381.7 to 391.3	43	64	S	Crystalline
391.3 to 400.7	56	56	S	Crystalline
400.7 to 409.3	46	52	S	Crystalline
409.3 to 418.6	45	58	S	Crystalline
418.6 to 427.8	43	60	S	Crystalline
427.8 to 437.2	38	58	S	Crystalline
437.2 to 446.4	38	58	S	Crystalline
446.4 to 455.9	46	60	S	Crystalline
455.9 to 465.2	35	60	S	Crystalline
465.2 to 474.4	170	70	S	Crystalline
474.4 to 483.8	169	70	S	Crystalline
483.8 to 493.5	169	62	S	Crystalline

Appendix B

Fracture Orientation Measurement Data from Drill Core 41-193.

Depth (Feet)	Strike	Dip	Direction	Comments
87.0 to 96.7	73	65	S	Crystalline
-	81	68	S	-
-	89	80	N	-
96.7 to 105.7	142	62	N	-
-	101	21	S	-
105.7 to 114.3	102	60	N	-
-	72	52	S	-
-	128	28	N	-
114.3 to 123.1	148	22	S	
-	156	26	S	-
-	176	52	S	-
-	170	52	S	-
-	56	55	S	-
-	62	46	S	-
-	172	30	S	-
123.1 to 131.8	74	28	S	-
-	58	42	S	-
-	60	40	N	
-	45	44	N	-
131.8 to 140.4	10	28	S	-
-	14	50	S	-
149.6 to 159.1	99	62	N	140.4 to 149.6 Brecciated
-	102	71	S	Crystalline
-	56	30	S	-
-	85	30	S	-
-	112	44	N	-
-	1	46	S	-
-	58	22	S	-
159.1 to 168.3	96	24	S	-
-	90	18	S	-
168.3 to 177.2	39	72	S	-
-	168	44	S	-
-	30	62	S	-
-	46	62	S	-
-	57	64	S	-
-	132	66	S	-
-	48	67	S	-
-	12	64	N	-
-	5	62	N	-

Depth (Feet)	Strike	Dip	Direction	Comments
177.2 to 186.3	4	50	S	Crystalline
-	49	70	S	-
-	159	48	S	-
177.2 to 186.3	179	28	N	Crystalline
-	36	72	S	-
-	10	56	S	-
186.3 to 195.2	87	40	S	-
-	111	80	N	-
-	168	42	N	-
-	132	30	N	-
-	26	48	S	-
-	89	56	N	-
-	117	80	N	-
-	135	79	N	-
-	2	24	N	-
-	54	24	N	-
-	17	21	S	-
-	76	72	N	-
-	144	88	N	-
-	80	15	S	-
-	83	42	S	-
-	159	50	S	-
-	8	28	S	-
-	40	70	S	-
195.2 to 204.6	12	58	S	-
-	16	20	S	-
-	148	35	N	-
-	14	60	S	-
204.6 to 214.0	60	62	N	-
-	154	64	S	-
-	19	64	S	-
-	95	30	N	-
-	175	19	S	-
-	20	10	S	-
-	27	12	S	-
-	80	22	S	-
214.0 to 223.0	83	32	S	-
-	23	42	S	-
-	74	64	S	-
-	11	38	S	-
251.1 to 260.5	37	38	S	223.0 to 251.1 Brecciated
-	36	38	S	Crystalline

Depth (Feet)	Strike	Dip	Direction	Comment
251 to 260.5	11	44	S	Crystalline
-	14	44	S	-
269.7 to 279.0	52	72	N	269.7 to 279.0 Brecciated
-	9	56	N	Crystalline
279.0 to 288.2	41	72	N	-
-	31	66	N	-
279.0 to 288.2	38	64	N	Crystalline
-	47	41	N	-
-	19	48	N	-
-	174	72	S	-
-	15	58	S	-
-	45	32	S	-
-	30	38	S	-
-	90	60	N	-
-	107	42	S	-
-	155	60	S	-
-	100	70	S	-
288.2 to 297.7	45	42	S	-
-	2	38	S	-
-	52	42	S	-
-	24	62	S	-
-	35	58	S	-
-	42	68	S	-
-	48	72	S	-
-	177	81	N	-
-	12	70	S	-
-	141	72	S	-
-	95	32	N	-
297.7 to 306.9	41	62	S	-
-	115	56	N	-
-	27	60	S	-
-	134	72	S	-
-	178	10	S	-
-	108	83	N	-
-	25	74	S	-
-	31	82	S	-
-	51	74	N	-
-	51	74	N	-
-	46	72	S	-
-	152	66	S	-
-	135	66	N	-
-	25	70	S	-

Depth (Feet)	Strike	Dip	Direction	Comments
306.9 to 316.1	160	72	S	Crystalline
-	91	78	N	-
-	41	62	S	-
-	158	68	S	-
-	36	50	S	-
-	151	58	S	-
-	170	60	S	-
-	95	60	N	-
-	28	58	S	-
316.1 to 325.7	149	62	N	Crystalline
-	79	72	S	-
-	136	46	S	-
-	159	84	N	-
-	2	68	S	-
-	162	56	N	-
-	159	46	N	-
-	138	48	N	-
-	61	80	S	-
-	37	78	S	-
325.7 to 335.1	140	50	S	-
-	20	32	N	-
-	43	68	S	-
-	47	78	N	-
-	159	78	N	-
-	149	62	N	-
-	99	26	S	-
-	123	33	N	-
-	175	68	N	-
-	138	58	N	-
-	167	80	N	-
-	119	48	S	-
-	147	42	S	-
-	27	34	S	-
-	20	30	S	-
-	159	80	S	-
-	159	80	S	-
-	149	70	N	-
-	30	78	S	-
335.1 to 344.3	133	70	S	-
-	76	20	S	-
-	133	80	S	-
-	135	54	N	-

Depth (Feet)	Strike	Dip	Direction	Comments
335.1 to 344.3	7	72	S	Crystalline
-	159	36	S	-
-	122	62	S	-
-	108	80	S	-
-	90	60	N	-
-	47	70	S	-
-	112	40	S	-
-	47	70	S	-
-	153	80	S	-
-	96	28	S	-
344.3 to 353.7	18	50	S	-
-	100	10	S	-
344.3 to 353.7	26	60	S	Crystalline
-	123	83	S	-
-	40	78	S	-
-	148	58	N	-
-	157	28	S	-
-	138	62	N	-
-	171	62	S	-
353.7 to 363.0	171	62	S	-
-	178	56	S	-
-	129	70	N	-
-	7	68	S	-
-	59	38	S	-
-	178	32	S	-
-	152	48	S	-
-	40	62	N	-
-	117	68	N	-
363.0 to 372.3	112	20	S	-
-	22	42	S	-
-	77	38	S	-
-	161	38	S	-
-	178	42	N	-
-	150	86	N	-
-	92	76	N	-
-	159	70	N	-
-	169	48	S	-
-	1	72	S	-
372.3 to 381.7	162	50	N	-
-	27	62	S	-
-	80	51	S	-
381.7 to 391.3	173	42	N	-

Depth (Feet)	Strike	Dip	Direction	Comments
381.7 to 391.3	102	48	S	Crystalline
-	105	70	S	-
-	159	70	N	-
-	105	50	S	-
-	73	50	N	-
391.3 to 400.7	38	68	S	-
-	177	45	N	-
-	101	48	S	-
-	160	60	N	-
-	18	68	S	-
-	59	70	S	-
400.7 to 409.3	92	50	S	-
-	22	78	S	-
-	35	80	S	-
-	152	80	S	-
400.7 to 409.3	108	42	S	Crystalline
-	34	78	S	-
-	35	80	S	-
-	120	78	N	-
-	140	50	S	-
409.3 to 418.6	4	38	N	-
-	174	55	N	-
-	144	58	S	-
-	154	58	N	-
-	123	56	S	-
-	20	68	S	-
-	58	70	S	-
418.6 to 427.8	88	68	S	-
-	144	70	N	-
-	14	72	N	-
-	105	80	N	-
-	111	86	S	-
-	127	60	N	-
-	3	58	N	-
-	28	60	S	-
-	155	60	N	-
427.8 to 437.2	17	64	N	-
-	49	50	S	-
-	41	62	S	-
-	44	86	S	-
-	19	54	S	-
-	19	54	S	-

Depth (Feet)	Strike	Dip	Direction	Comments
427.8 to 437.2	56	74	S	Crystalline
-	19	80	S	-
-	118	80	N	-
-	43	86	N	-
-	29	62	N	-
437.2 to 446.4	1	52	N	-
-	42	82	N	-
-	42	82	N	-
-	42	82	N	-
-	40	60	S	-
446.4 to 455.9	109	60	S	-
-	174	72	S	-
-	120	54	S	-
-	132	82	N	-
-	150	74	S	-
-	174	50	N	-
-	150	45	S	-
-	135	68	S	-
455.9 to 465.2	120	54	S	Crystalline
-	56	72	N	-
-	88	48	S	-
-	175	38	N	-
-	68	42	S	-
-	22	70	S	-
465.2 to 474.4	85	72	S	-
-	38	60	N	-
-	45	74	N	-
-	102	64	S	-
-	165	72	S	-
-	5	50	S	-
-	169	66	N	-
-	38	63	S	-
-	159	62	N	-
-	79	68	S	-
474.4 to 483.8	159	62	N	-
-	125	70	S	-
-	72	56	S	-
-	37	76	S	-
-	31	72	S	-
-	36	62	N	-
-	4	64	N	-

Depth (Feet)	Strike	Dip	Direction	Comments
474.4 to 483.8	3	89	S	Crystalline
-	159	64	S	-
-	2	62	N	-
-	115	72	N	-
-	172	32	N	-
-	170	30	N	-
-	149	58	N	-
483.8 to 493.5	6	64	N	-
-	4	34	N	-
-	8	32	S	-
-	152	58	N	-
-	162	56	N	-
-	162	40	N	-
-	20	56	S	-
-	51	78	S	-
-	118	50	N	-
-	170	60	N	-

Appendix C

Foliation Orientation Measurement Data from Drill Core 41-190.

Depth (Feet)	Strike	Dip	Direction	Comments
35.0 to 44.0	96	40	S	Crystalline
230.8 to 240.3	22	56	N	44.0 to 230.8 Brecciated
268.0 to 277.6	41	58	S	240.3 to 268.0 Split
305.5 to 314.9	40	64	S	277.6 to 305.5 Unoriented
314.9 to 324.3	34	62	S	Crystalline
324.3 to 333.7	50	54	N	Crystalline
333.7 to 343.0	46	64	N	Crystalline
446.4 to 455.8	17	72	S	343.0 to 446.4 Split
445.8 to 465.2	30	80	S	Crystalline
465.2 to 474.4	174	72	S	Crystalline
474.4 to 483.5	17	80	S	Crystalline
483.5 to 492.7	20	80	S	Crystalline
492.7 to 502.0	36	78	S	Crystalline
502.0 to 511.6	58	62	S	Crystalline
511.6 to 521.3	19	78	S	Crystalline
521.3 to 530.9	38	70	S	Crystalline
530.9 to 540.2	36	86	S	Crystalline
540.2 to 549.4	15	60	S	Crystalline
549.4 to 558.7	22	66	S	Crystalline
558.7 to 567.9	21	67	S	Crystalline
567.9 to 575.2	15	56	S	Crystalline
575.2 to 586.5	45	60	S	Crystalline
586.5 to 595.8	42	62	S	Crystalline
595.8 to 605.4	47	68	S	Crystalline
605.4 to 614.5	60	64	S	Crystalline
614.5 to 624.0	52	62	S	Crystalline
624.0 to 633.2	43	64	S	Crystalline
633.2 to 642.8	56	56	S	Crystalline
642.8 to 651.9	46	52	S	Crystalline
651.9 to 661.3	45	58	S	Crystalline
661.3 to 670.7	43	60	S	Crystalline
670.7 to 680.2	38	58	S	Crystalline
680.2 to 689.6	38	58	S	Crystalline
689.6 to 698.8	46	60	S	Crystalline

Appendix D

Fracture Orientation Measurement Data from Drill Core 41-190.

Depth (Feet)	Strike	Dip	Direction	Comments
35.0 to 44.0	80	62	S	Crystalline
-	122	48	S	-
-	16	44	S	-
-	18	64	S	-
-	49	66	N	-
44.0 to 53.3	177	68	S	-
-	103	55	S	-
-	129	38	S	-
-	115	45	S	-
-	116	38	S	-
-	63	59	S	-
-	88	64	S	-
-	153	46	S	-
-	9	60	S	-
53.3 to 63.0	154	32	S	-
63.0 to 72.5	22	60	S	-
-	25	75	S	-
-	2	65	S	-
-	2	65	S	-
72.5 to 81.8	1	60	S	-
-	27	55	S	-
-	38	66	S	-
-	42	56	S	-
-	10	76	S	-
81.8 to 91.2	145	76	S	-
-	3	76	S	-
-	0	82	E	-
91.2 to 101.0	48	68	S	-
-	74	82	S	-
101.0 to 110.4	9	32	N	-
110.4 to 121.0	99	80	S	-
-	28	52	S	-
-	27	56	S	-
121.0 to 129.1	13	52	S	-
-	74	63	N	-
129.1 to 138.8	17	42	S	-
-	42	60	S	-
138.8 to 147.9	27	58	S	-
-	129	86	N	-
-	122	80	N	-
-	122	80	N	-

Depth (Feet)	Strike	Dip	Direction	Comments
147.9 to 157.1	32	64	N	Crystalline
-	32	64	N	-
-	62	60	N	-
-	47	58	N	-
-	0	54	E	-
157.1 to 163.0	28	44	S	Crystalline
-	17	40	S	-
-	86	68	N	-
-	84	-68	N	-
-	19	40	S	-
-	33	56	S	-
-	70	40	S	-
230.8 to 240.3	166	66	N	163.0 to 240.3 Unoriented
-	27	46	S	Crystalline
-	158	58	S	-
-	168	74	S	-
-	176	86	N	-
268.0 to 277.6	46	62	S	240.3 to 268.0 Split
-	124	80	S	Crystalline
-	166	50	S	-
-	110	70	S	-
-	63	78	N	-
-	100	70	N	-
305.5 to 314.9	50	25	S	277.6 to 305.5 Unoriented
-	67	64	S	Crystalline
-	37	58	S	-
-	87	60	S	-
-	117	75	S	-
-	53	74	S	-
-	80	62	S	-
-	80	80	S	-
-	89	78	S	-
-	9	82	S	-
-	168	48	S	-
-	96	68	S	-
-	165	50	S	-
-	18	60	S	-
-	88	62	S	-
-	17	42	S	-
-	1	60	S	-
-	124	58	S	-
-	100	58	S	-
-	115	54	S	-

Depth (Feet)	Strike	Dip	Direction	Comments
305.5 to 314.9	37	55	S	Crystalline
-	23	62	S	-
-	43	57	S	-
-	129	82	S	-
314.9 to 324.3	44	58	N	-
-	123	80	N	-
-	43	45	N	-
-	16	82	N	-
-	147	80	S	-
-	35	68	S	-
-	144	62	S	-
-	0	62	E	-
324.3 to 333.7	149	78	S	Crystalline
-	152	80	S	-
-	99	48	N	-
-	147	78	S	-
-	150	82	S	-
-	8	80	S	-
-	59	70	N	-
333.7 to 343.0	136	42	N	-
-	154	52	N	-
-	53	72	S	-
-	49	64	S	-
-	48	74	S	-
-	122	58	S	-
-	15	82	S	-
-	128	72	S	-
-	102	60	S	-
-	36	58	S	-
-	162	82	S	-
446.4 to 455.8	49	64	S	343.0 to 446.4 Split
445.8 to 465.2	175	48	S	Crystalline
-	35	50	S	-
-	81	40	S	-
-	175	52	S	-
-	130	80	S	-
-	145	72	S	-
-	40	72	S	-
-	154	80	S	-
-	152	62	S	-
-	178	56	N	-
465.2 to 474.4	118	50	S	-
-	148	84	S	-
-	148	84	S	-
474.4 to 483.5	24	64	S	-
-	8	56	N	-

Depth (Feet)	Strike	Dip	Direction	Comments
474.4 to 483.5	0	45	E	Crystalline
-	171	70	S	-
-	25	56	S	-
483.5 to 492.7	8	56	N	-
-	39	42	N	-
492.7 to 502.0	99	70	N	-
-	49	82	S	-
-	65	52	S	-
-	58	66	S	-
502.0 to 511.6	66	54	N	-
-	70	70	S	-
-	140	82	N	-
-	153	84	S	-
-	60	62	N	-
511.6 to 521.3	70	78	S	-
-	0	56	S	-
511.6 to 521.3	46	46	S	Crystalline
-	145	40	N	-
521.3 to 530.9	125	76	S	-
-	129	80	S	-
530.9 to 540.2	58	66	S	-
-	36	82	S	-
-	36	80	S	-
540.2 to 549.4	0	58	E	-
-	50	58	S	-
-	50	58	S	-
-	50	58	S	-
-	154	84	S	-
-	160	80	S	-
-	92	86	S	-
549.4 to 558.7	0	38	E	-
-	55	62	N	-
-	118	70	N	-
-	173	70	N	-
-	136	76	S	-
-	30	60	S	-
-	32	52	S	-
-	40	42	S	-
-	33	76	S	-
558.7 to 567.9	100	72	S	-
-	162	66	N	-
-	127	83	S	-
567.9 to 575.2	127	83	S	-
-	162	66	N	-
-	138	78	N	-
-	171	55	S	-

Depth (Feet)	Strike	Dip	Direction	Comments
567.9 to 575.2	38	66	S	Crystalline
-	136	82	S	-
-	36	80	S	-
-	57	78	S	-
-	47	76	S	-
575.2 to 586.5	40	70	S	-
-	0	26	E	-
-	116	62	S	-
-	131	18	S	-
586.5 to 595.8	34	90	S	-
-	65	62	S	-
-	39	64	S	-
-	62	63	S	-
-	154	50	S	-
-	36	66	S	-
-	58	78	N	-
-	30	68	S	-
-	47	60	S	-
595.8 to 605.4	32	62	S	-
-	81	58	S	-
595.8 to 605.4	50	68	S	Crystalline
-	44	60	S	-
605.4 to 614.5	62	72	S	-
-	62	72	S	-
-	62	72	S	-
-	30	50	S	-
-	66	68	S	
-	66	68	N	-
-	147	78	N	-
-	46	78	S	-
614.5 to 634.0	77	76	S	-
-	56	66	S	-
-	39	60	S	-
-	105	60	S	-
-	39	58	S	-
-	59	50	N	-
-	46	55	N	-
-	46	55	N	-
624.0 to 633.2	32	70	S	-
-	113	66	S	-
-	57	54	S	-
-	28	74	S	-
-	110	42	S	-
-	53	58	S	-
633.2 to 642.8	42	54	S	-

Depth (Feet)	Strike	Dip	Direction	Comments
633.3 to 642.8	120	80	N	Crystalline
-	55	58	S	-
-	114	56	S	-
642.8 to 651.9	35	59	S	-
-	89	52	S	-
-	40	41	S	-
-	130	50	S	-
651.9 to 661.3	28	70	S	-
-	133	60	N	-
-	19	48	S	-
-	46	54	S	-
-	14	74	S	-
661.3 to 670.7	63	59	S	-
-	38	56	S	-
-	79	68	S	-
-	59	73	S	-
-	105	50	N	-
-	70	60	S	-
-	62	68	S	-
-	59	56	S	-
670.7 to 680.2	50	70	S	-
-	75	70	N	-
-	17	74	S	-
-	50	70	S	-
680.2 to 689.6	109	80	N	-
680.2 to 689.6	90	80	N	Crystalline
-	31	56	S	-
689.6 to 698.8	34	50	S	-
-	51	62	S	-
-	47	54	S	-
-	65	56	S	-
-	24	61	S	-

Appendix E

Fracture Orientation Measurement Data from Drill Core 57-27 (Whole).

Depth (Feet)	Strike	Dip	Direction	Comments
221.9 to 230.9	130	69	S	Triassic
-	142	72	S	-
-	86	80	N	-
-	99	82	S	-
-	129	80	N	-
-	88	80	N	-
-	85	80	N	-
-	139	72	S	-
-	78	62	S	-
230.9 to 240.5	35	46	N	-
-	155	66	S	-
-	155	72	S	-
-	155	70	S	-
-	55	60	N	-
-	56	60	N	-
240.5 to 249.8	76	69	S	-
880.0 to 897.1	40	30	S	249.8 to 880.0 Unoriented
-	72	66	S	Crystalline
-	64	56	S	-
897.1 to 906.7	78	79	S	-
-	74	78	S	-
-	80	70	S	-
-	122	86	N	-
-	100	80	S	-
-	126	80	N	-
-	114	69	S	-
-	112	80	S	-
906.7 to 915.9	110	78	N	-
-	124	80	N	-
-	116	80	N	-
-	53	60	S	-
-	109	78	N	-
-	100	65	N	-
-	104	70	N	-
-	110	70	N	-
-	110	60	S	-
-	70	70	S	-
934.5 to 949.1	67	76	S	915.9 to 934.5 Split
-	85	76	S	Crystalline

Depth (Feet)	Strike	Dip	Direction	Comments
944.1 to 953.4	49	66	S	Crystaline
-	76	66	S	-
-	146	78	N	-
-	134	70	S	-
944.1 to 953.4	146	80	N	Crystalline
953.4 to 963.0	66	56	S	-
953.4 to 963.0	60	56	S	Crystalline
-	120	78	N	-
-	84	60	S	-
-	104	86	S	-
990.8 to 1000.0	74	50	S	963.0 to 990.8 Unoriented
-	102	54	S	Crystalline
-	76	54	S	-
-	86	20	N	-
-	120	80	S	-
-	66	74	S	-
1000.0 to 1009.7	18	76	N	-
-	171	70	N	-
-	75	54	S	-
-	116	70	S	-
1009.7 to 1018.5	75	64	S	-
-	38	64	S	-
-	44	50	S	-
1027.8 to 1037.0	148	65	S	1018.5 to 1027.8 Missing Box
-	152	65	S	Crystalline
-	149	65	S	-
-	119	65	S	-
-	186	70	S	-
-	130	72	S	-
1037.0 to 1046.4	105	62	S	-
-	61	42	N	-
-	63	44	N	-
-	38	78	S	-
-	167	68	S	-
1046.4 to 1055.8	79	80	S	-
-	90	86	S	-
-	88	84	S	-

Appendix F

Fracture Orientation Measurement Data from Outcrop GTA 894.

Strike
106
136
108
103
142
118
126
147
10
120
122
122
122
140
128
128
128
136
130
12
130
125
129
135
137
147
102
166
145
134
128
124
124
120
128
128
116
116
109
119
74

Strike
12
127
163
136
127
127
142
132
129
0
126
130
133
132
155
6
21
14
23
32

Appendix G

Fracture Orientation Measurement Data from Outcrop SPG 223.

Window 1

Strike
129
124
105
120
55
114

Window2

Strike
129
129
129
115
123
117
165
137
127
105
105
111
103
97
124
2
2
109
109

Window 3

Strike
138
148
121
132
140
128
124
126
122
124
124
127
127
122
128
150
136
131
131
161
131
124
124
124

Window 4

Strike
149
121
139
155
139
129
122
138
142
142
145
159
145
129
138
127
122
128
124
124
124
124
124
124
124
129
129
129
140
140
120

Window 5

Strike
22
5
169
148
151
145

Window 6

Strike
136
132
132
107
141
141
141
141
112
108

Appendix H

Fracture Orientation Measurement Data from Outcrop SPG 231.

Strike
120
118
119
121
120
120
120
120
120
120
120
120
120
120
120
120
119
119
120
120
120
120
120
120
120
120
119
119
120
120
120
125
125
125
125
125
125
125
125
125
120
120
120
120
120

Strike
36
38
36
38
30
120
120
120
120
120
120
120
120
120
120
120
120
120
120
120
119
120
38
36
120
119
120
38
36
119
120
120
120
119
120
119
120
38
36
35
120
119
120

Strike
38
38
80

Appendix I

Fracture Orientation Measurement Data from Outcrop SPG 311.

Strike
130
38
125
130
122
130
124
130
125
124
123
40
38
37
130
126
128
130
130
130
125
125

Strike
125
123
130
70
70
68
125
130
128
125
130
130
130
130
125
122
124
130
130
130
125
123
125

Appendix J

Fracture Orientation Measurement Data from Outcrop MA 771.

Strike
120
125
162
130
175
120
125
130
125
165
125
120
120
130
125
156
130
120
125
130